Supporting Information

Ladder-Type Phenazine-Linked Covalent Organic Polymers with Synergistic Cation-π Interactions for Highly Stable Lithium Metal Batteries

Xiao-Meng Lu,‡ Haichao Wang,‡ Yiwen Sun, Yi Xu, Yang Wu, Weiwei Sun, Chao Yang, Yifan Zhang, and Yong Wang *

Department of Chemical Engineering, School of Environmental and Chemical Engineering, Shanghai University, 99 Shangda Road, Shanghai 200444, People's Republic of China

‡These authors contributed equally to this work.

*Corresponding authors: Tel: +86-21-66137723; fax: +86-21-66136116.
Email address: yongwang@shu.edu.cn (Y. Wang).

Experimental Section

Materials: Cyclohexanehexone octahydrate (CHH-M, 99%) and 1,2-Phenylenediamine (PD-M, 99%) was purchased from Aladdin. 2,3,7,8-Phenazinetetramine, hydrochloride (2:3) (PT-M, 97%) were purchased from Henan Psai Chemical Products Co., Ltd. Methanol (CH_4O, abbreviated as MeOH, >99.5%), ethyl alcohol (C_2H_6O, abbreviated as EtOH, >99.7%), acetone (C_3H_6O, abbreviated as AC, ≥99.5%), acetic acid ($C_2H_4O_2$, abbreviated as AcOH, ≥99.0%), tetrahydrofuran (C_4H_8O, abbreviated as THF, ≥99.0%),1,4-dioxane ($C_4H_8O_2$, abbreviated as 1,4-Diox, ≥99.5%), 1,2,4-Trimethylbenzene (C_9H_{12}, abbreviated as TMB, ≥98.0%), and N-Methylpyrrolidone (C_5H_9NO, abbreviated as NMP, ≥99.0%) were obtained from Sinopharm Chemical Reagent Co., Ltd. All relevant starting materials, solvents were purchased from a commercial source and used without further purification.

Preparation of PZ-CHPD: A mixture of 780 mg of CHH-M and 870 mg of PD-M was prepared in a 250 mL round-bottom flask with 50 mL of anhydrous MeOH. The round-bottom flask was then heated in an oil bath at 105 °C for 8 h. Once cooled to room temperature, the precipitate was collected by centrifugation and washed repeatedly with EtOH, AC, and THF. The product was then dried overnight under vacuum at 60 °C.

Preparation of PZ-CHPT: A mixture of 31.2 mg of CHH-M, 57.4 mg of PT-M, 3 mL of TMB, 3 mL of 1,4-Diox, and 0.6 mL of a 6 M AcOH solution was prepared in a

10 mL Pyrex tube and sonicated for 10 min. The tube was initially evacuated, then filled with Ar gas, and this process was repeated 3 times. The tube was then heated in an oven at 150 °C for 4 days. After cooling to room temperature, the precipitate was collected by centrifugation and washed with EtOH, AC, and THF. The product was then dried under vacuum at 60 °C overnight.

Preparation of Li@PZ-CHPT: 1 mg of PZ-CHPT powder was dispersed in 1 mL of NMP and subjected to ultrasonication for 30 minutes to produce a 1 mg mL^{-1} PZ-CHPT@NMP suspension. Then, 30 μL of the PZ-CHPT@NMP suspension was applied onto a 12 mm diameter Li foil. Finally, the Li foils were dried under vacuum at room temperature in a glove box to obtain Li@PZ-CHPT.

Preparation of Cu@PZ-CHPT: The PZ-CHPT was mixed with PVDF in a 9:1 weight ratio in the NMP solution. The thoroughly mixed slurry was applied to a 12 mm diameter copper (Cu) foil. The Cu@PZ-CHPT electrodes were prepared by drying overnight at 60 °C under vacuum.

Preparation of $LiFePO_4$ (LFP) cathode: For LFP cathode fabrication, commercial LFP powder was combined with Super P carbon and PVDF in a weight ratio of 8:1:1, using NMP as the solvent. The slurry was then applied to a 12 mm diameter Al foil and dried in a vacuum oven at 60 °C for 12 h, achieving an average mass loading of 2-4 mg cm^{-2}.

Characterization: Scanning electron microscopy (SEM, Hitachi SU1510) and transmission electron microscopy (TEM, Hitachi HT7820), along with corresponding elemental distribution analysis, were employed to examine the morphology of PZ-CHPT and PZ-CHPD. To evaluate the structure and phase of PZ-CHPT and PZ-CHPD, X-ray diffraction (XRD) measurements were conducted on a Bruker D8 Advance diffractometer, with a voltage of 40 kV and a current of 40 mA. Fourier transform infrared (FT-IR) spectra of PZ-CHPT and PZ-CHPD were obtained with a Nicolet 380 FT-IR spectrometer. Raman spectra (Raman, Renishaw in via Plus) were employed to study the organic groups in the two phenazine-based COPs. The chemical state of surface compositions of PZ-CHPT and PZ-CHPD was performed using a Thermo Scientific™ K-Alpha™ spectrometer. Thermogravimetric analysis (TGA, NETZSCH TG 209 F1 Libra) was conducted in an N_2 atmosphere at a heating rate of 10 °C min^{-1} to assess the stability of the two phenazine-based COPs. The commercial Bruker Multimode 8 with Nanoscope V controller was implemented in the PeakForce Quantitative Nano-Mechanics mode for performing Atomic Force Microscope (AFM, Dimension Icon) investigations. BET surface areas were determined using a Micromeritics ASAP 2020M+C analyzer and N_2 adsorption/desorption isotherms obtained at 77 K. *In situ* optical image (OM) investigations were carried out using the Zeiss Smartzoom 5.

Electrochemical measurements: The asymmetric, symmetric cells of Li||PZ-

CHPD@Cu and Li@CHPT||Li@CHPT were fabricated using CR2032 coin cells, a commercial Clegard 2400 polypropylene separator, and 40 μL of a 1.0 M LiTFSI solution in a 1:1 (v/v) mixture of DOL and DME, with 0.2 M $LiNO_3$ added as the electrolyte. Meanwhile, the full cells of Li@PZ-CHPT|LFP used 40 μL of a 1 M $LiPF_6$ solution in EC/DEC (1:1 w/w) as the electrolyte. The voltage range of the full cells was set between 2.5 and 4.2 V at different current densities. The cyclic electrochemical tests were carried out on a Land CT2001A electrochemical testing system. The electrochemical impedance spectra of Li@CHPT||Li@CHPT symmetric cells, with frequencies ranging from 100 kHz to 0.01 Hz, were recorded using a CHI660E Electrochemical Workstation (Shanghai Chenhua Instrument).

Theoretical calculation: For all calculations in this work, density functional theory (DFT) was applied using the DMOL^3 code in Materials Studio.[1] The calculations were carried out within the framework of density functional theory using the Perdew-Burke-Ernzerhof (PBE) functional, based on the generalized gradient approximation (GGA).[2] To account for relativistic effects, the All-Electron Relativistic approach was employed, which considers all electrons and integrates relativistic effects into the core.[3] The double numerical atomic orbital basis set, augmented with a polarization function (DNP), was selected. For the geometry structural optimization, the convergence criteria for energy, maximum force, and displacement were specified at 'fine' quality, with values of 1×10^{-5} Ha, 2×10^{-3} Ha/Å, and 5×10^{-3} Å, respectively.

For the pair PZ-CHPT and Li^+, the adsorption energy is calculated using the

equation provided below:

Eabs = $E_{Li+PZ-CHPT} - E_{PZ-CHPT} - E_{Li}$, where $E_{Li+PZ-CHPT}$, $E_{PZ-CHPT}$, and E_{Li} refer to the optimized energies of the PZ-CHPT with an adsorbed Li atom, PZ-CHPT segment model, and isolated Li atom, respectively.

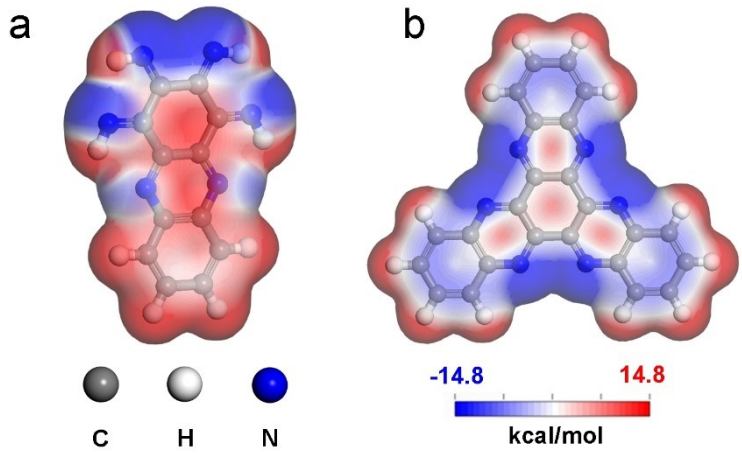

Fig. S1 Simulated ESP distribution of (a) PZ-CHPD and (b) PZ-CHPT. Notes: blue represents the electronegative regions, while red indicates the electropositive regions.

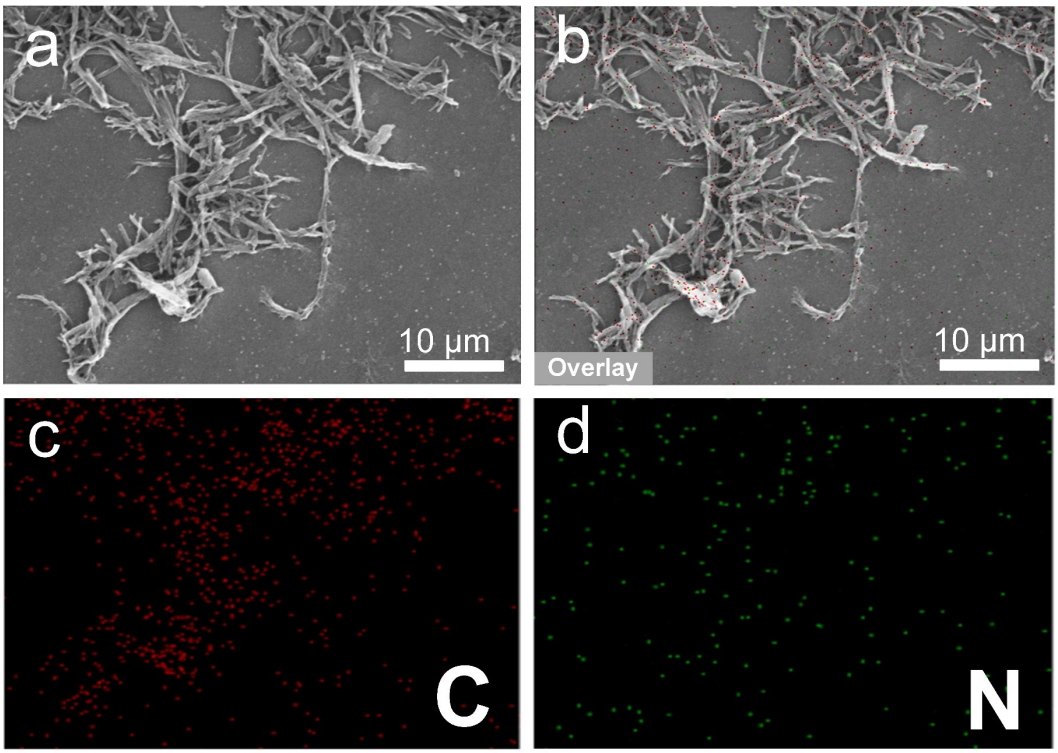

Fig. S2 (a) SEM and (b-d) EDS images of PZ-CHPD.

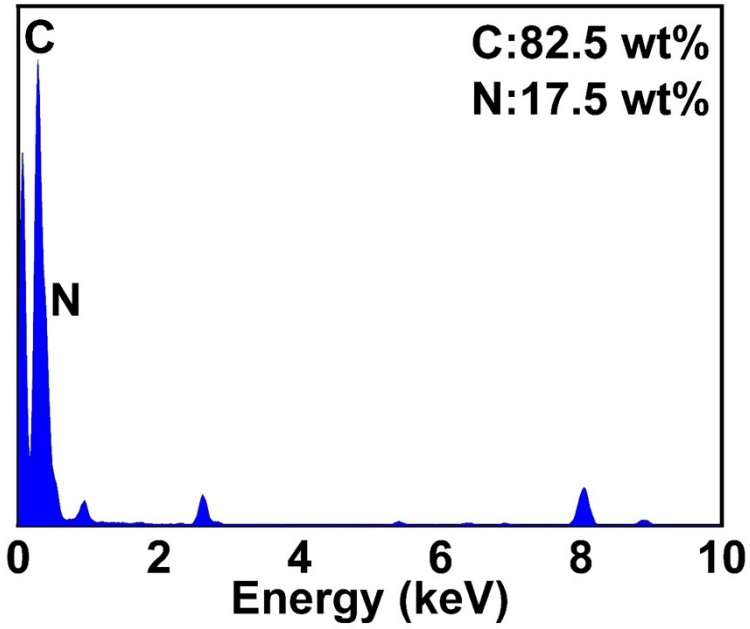

Fig. S3 EDX patterns of PZ-CHPT.

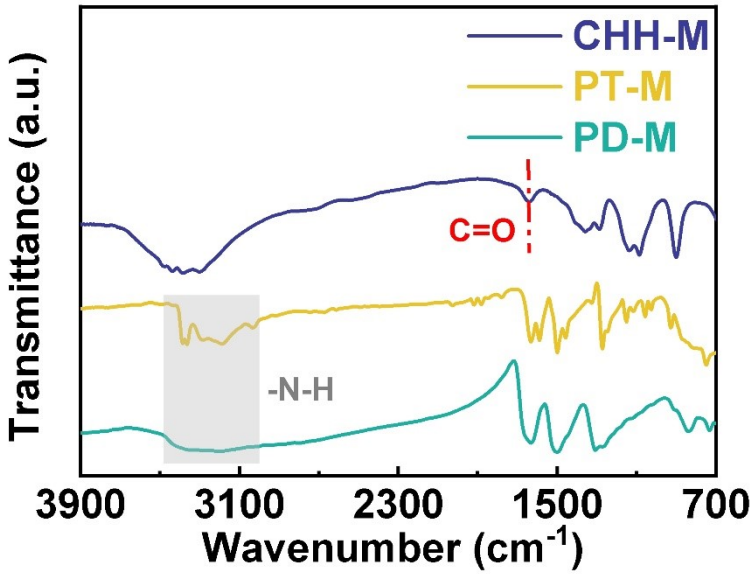

Fig. S4 FT-IR spectra of CHH-M, PT-M and PD-M monomers.

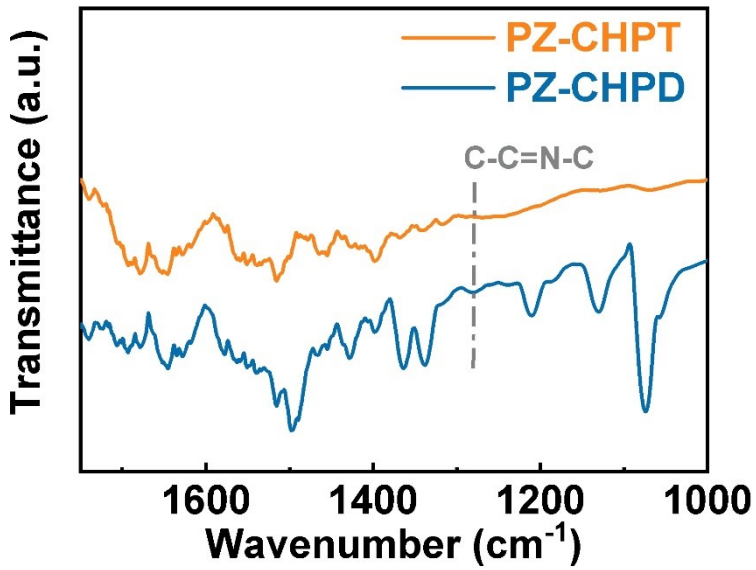

Fig. S5 FT-IR spectra of PZ-CHPT and PZ-CHPD products.

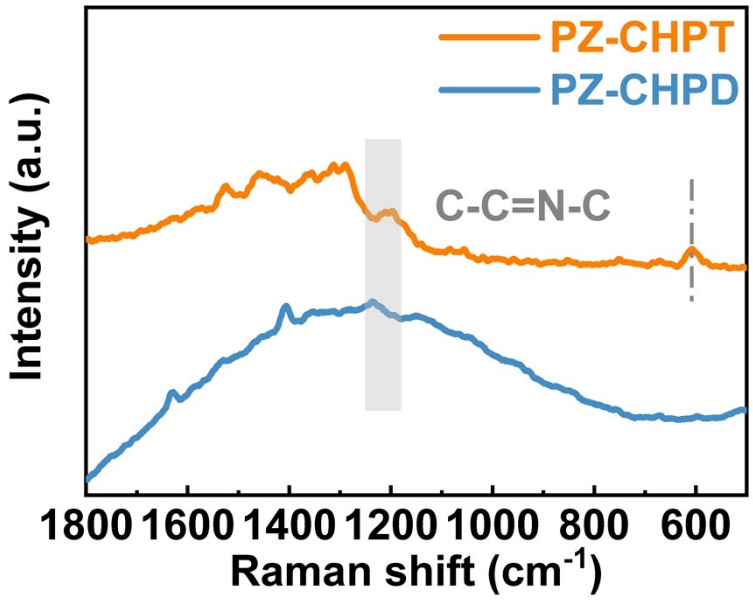

Fig. S6 Raman spectra of PZ-CHPT and PZ-CHPD products.

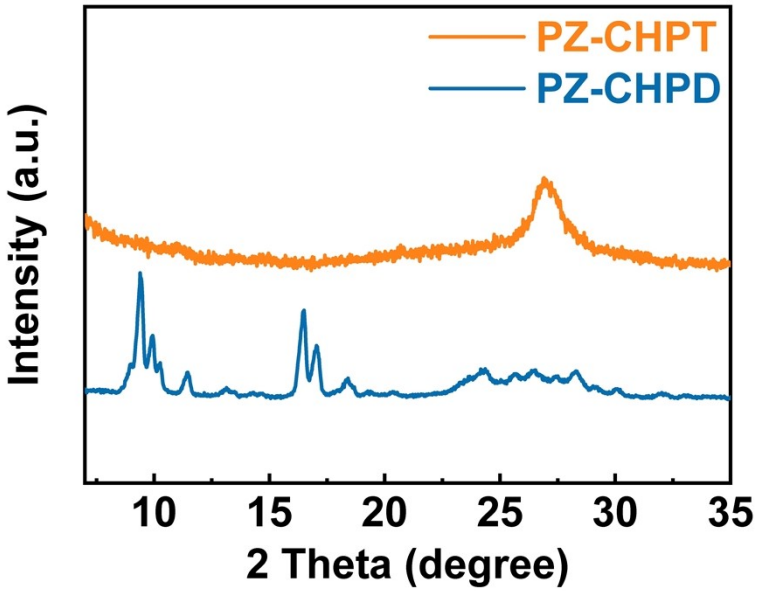

Fig. S7 PXRD patterns of the synthesized PZ-CHPT and PZ-CHPD. The pattern demonstrates the short-range ordering of PZ-CHPT.

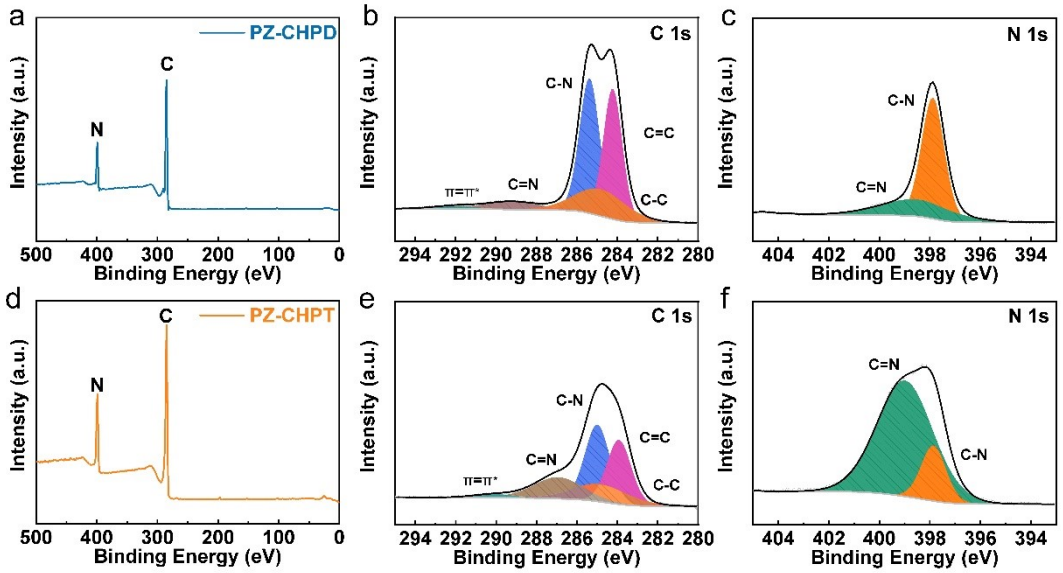

Fig. S8 XPS survey spectra of (a) PZ-CHPD, (d) PZ-CHPT. High-resolution XPS spectra of C 1s for (b) PZ-CHPD, (e) PZ-CHPT. High-resolution XPS spectra of N 1s for (c) PZ-CHPD, (f) PZ-CHPT. As shown in Figure S7a and S7d, the XPS survey spectra show that both the phenazine-based products exhibited two peaks corresponding to C and N elements. The high-resolution C 1s spectrum shown in Figure S7b and S7e, peaks at 286.8, 285.4, 284.8 and 283.8 eV are associated with C=N, C-N, C-C and C=C signals, respectively.[4] Similarly, in the high-resolution N 1s spectrum (Figure S7c and S7f), the peaks at 399.9 eV and 398.6 eV are associated with C−N and C=N signals, respectively.[5]

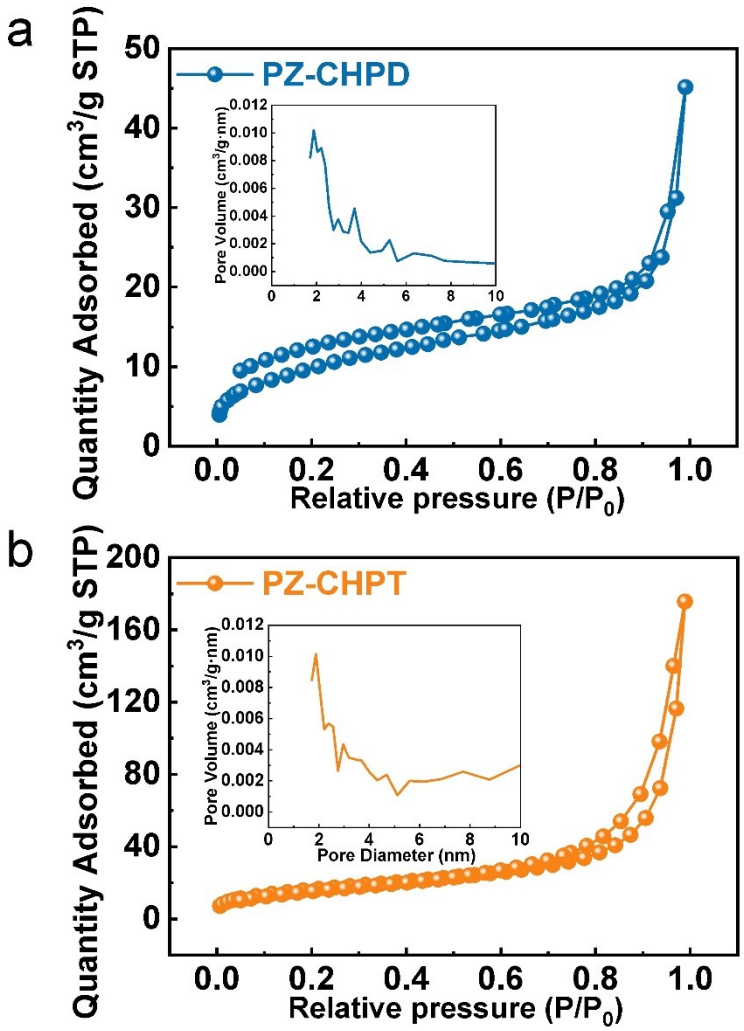

Fig. S9 N_2 adsorption−desorption isotherm and inset revealing pore size distributions of (a) PZ-CHPD and (b) PZ-CHPT. Based on the N_2 adsorption isotherm, PZ-CHPD and PZ-CHPT have average pore sizes of 7.72 nm and 18.35 nm, respectively.

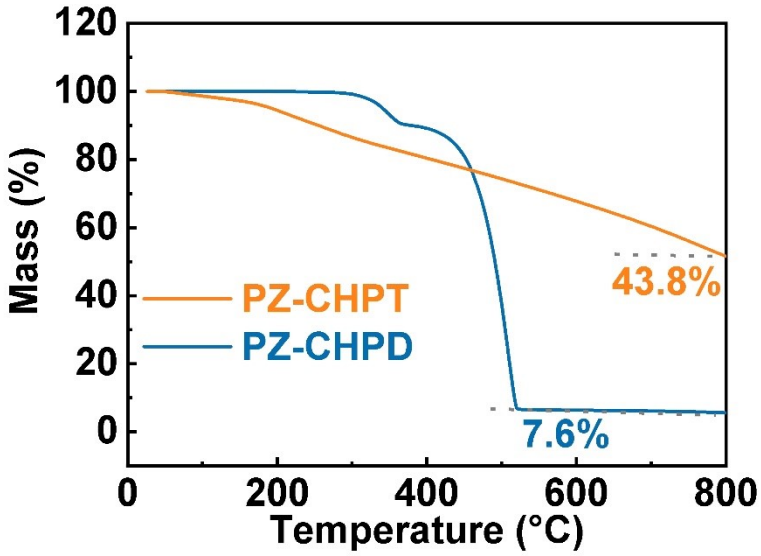

Fig. S10 TGA curves of PZ-CHPD and PZ-CHPT products in N_2 atmosphere with the heating rate of 10 ℃ min^{-1}.

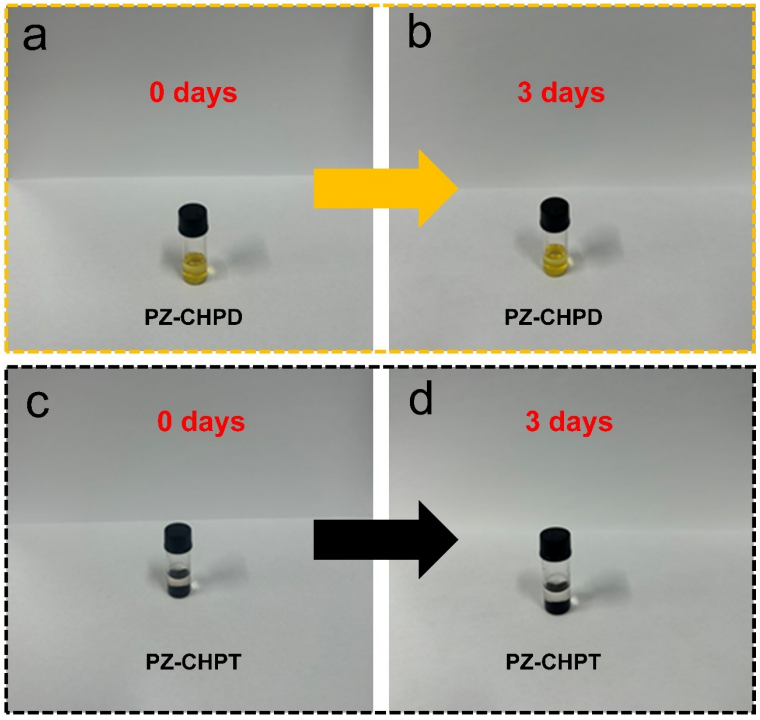

Fig. S11 Solubility of the PZ-CHPD sample in the electrolyte for (a) 0 day and (b) 3 days. Solubility of the PZ-CHPT sample in the electrolyte for (c) 0 day and (d) 3 days.

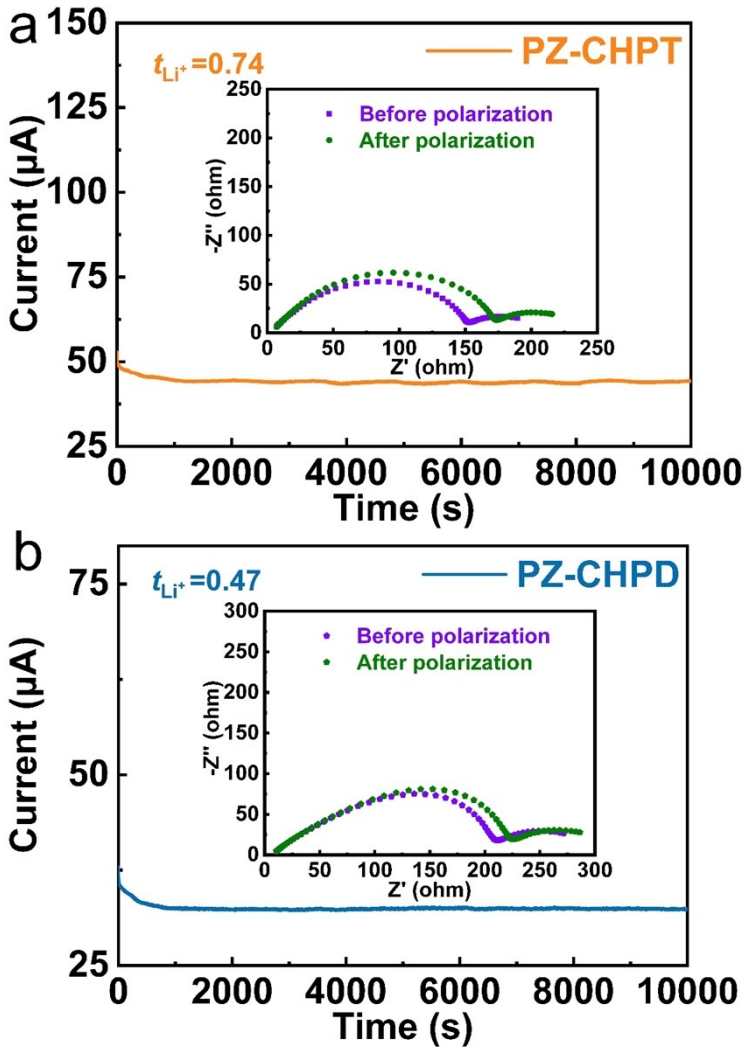

Fig. S12 Polarization curve and impedance diagram of symmetric cells before and after polarization (constant potential: 10 mV) for (a) Li@PZ-CHPT||Li@PZ-CHPT and (b) Li@PZ-CHPD||Li@PZ-CHPD.

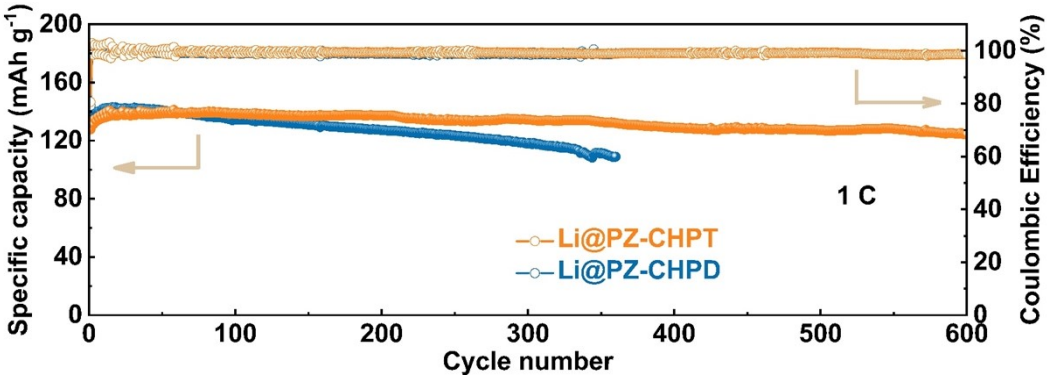

Fig. S13 Cycling performance of Li@PZ-CHPT||LFP and Li@PZ-CHPD||LFP full batteries at 1 C.

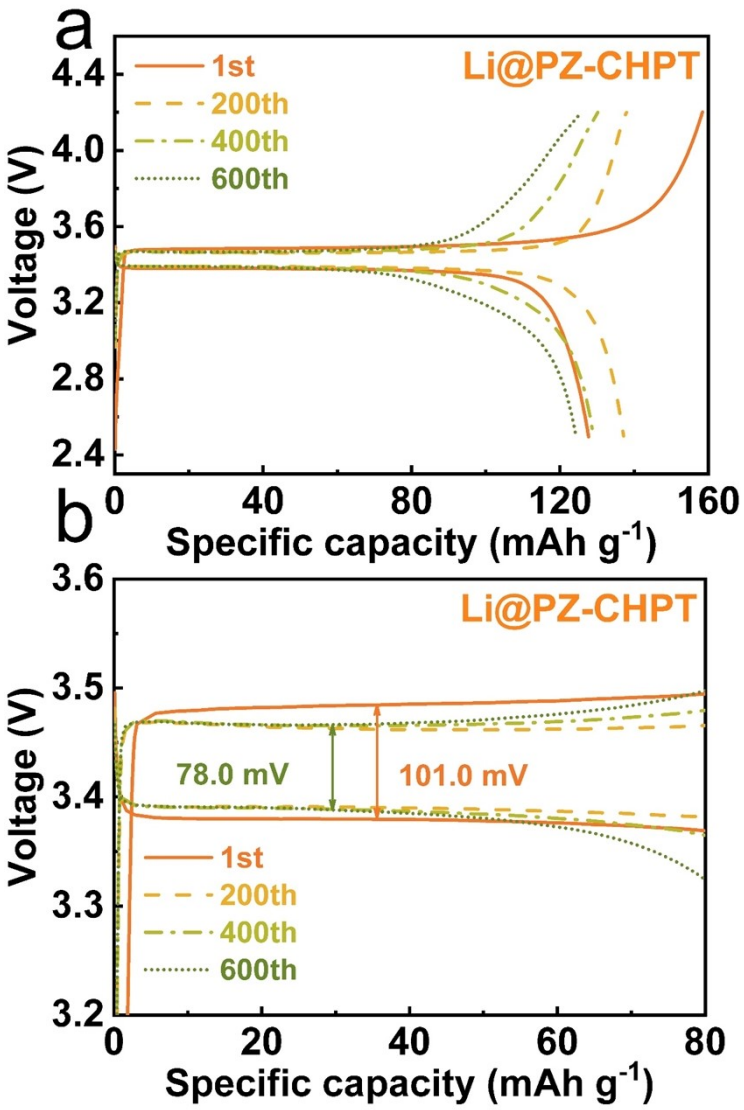

Fig. S14 (a, b) Galvanostatic charge−discharge curves of Li@PZ-CHPT||LFP full cells at 1 C.

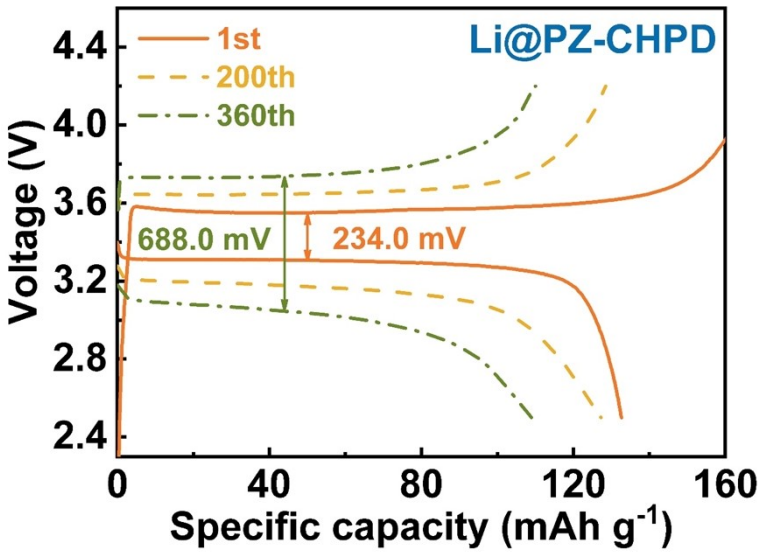

Fig. S15 Galvanostatic charge−discharge curves of Li@PZ-CHPD||LFP full cells at 1 C.

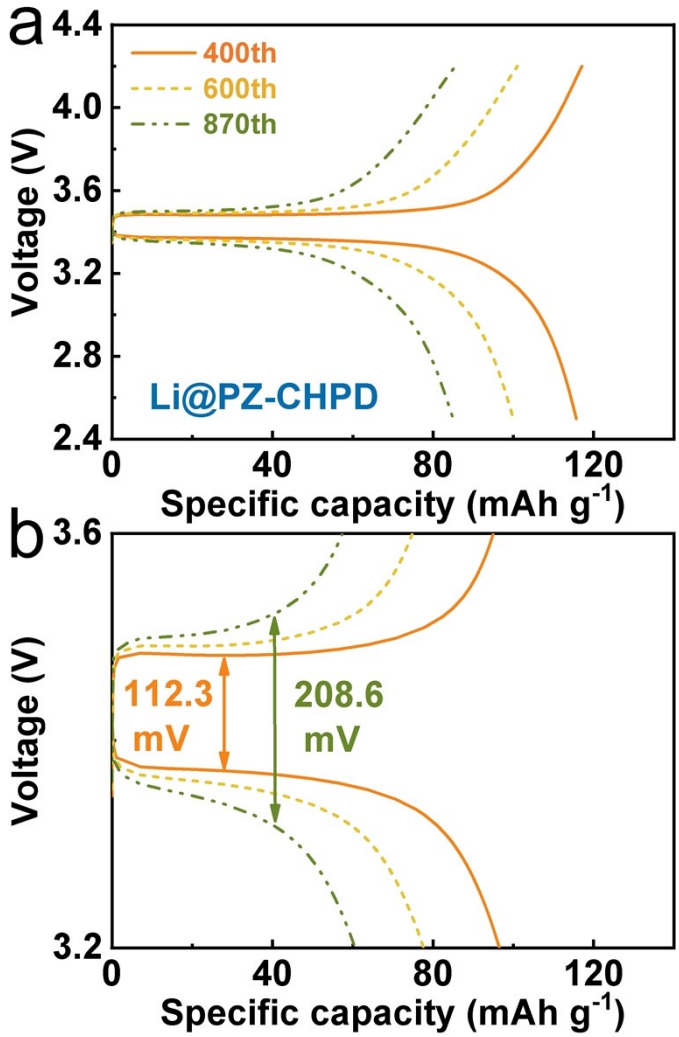

Fig. S16 Galvanostatic charge−discharge curves of Li@PZ-CHPD||LFP full cells at 3 C.

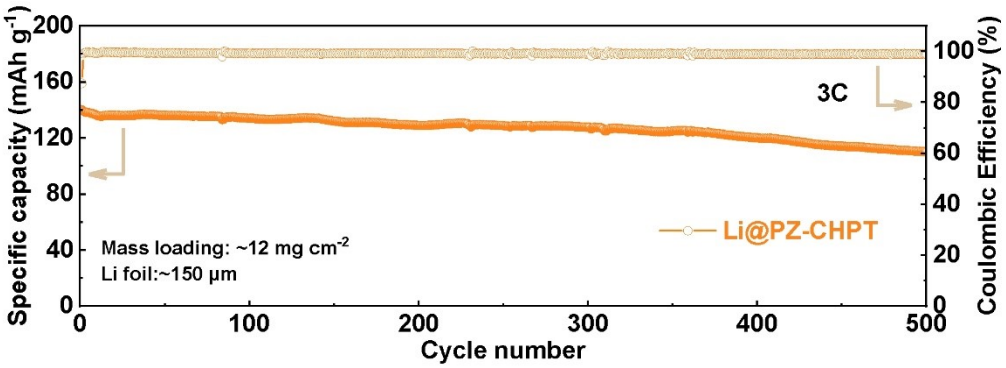

Fig. S17 Cycling performance of Li@PZ-CHPT||LFP full cells with high-loading cathode (~12 mg cm^{-2}) and thin Li foil (~150 μm) at 3 C.

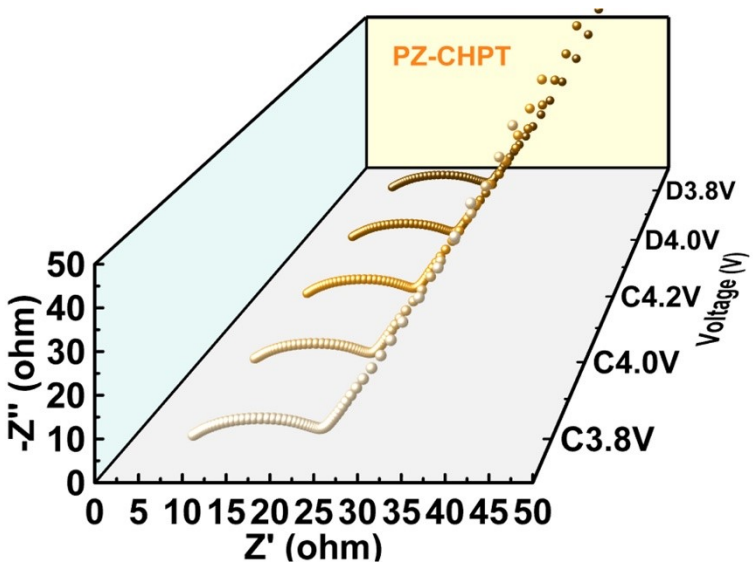

Fig. S18 EIS of Li@PZ-CHPT||LFP full cells at at different states of charge. The interfacial impedance plays a key role in regulating Li flux; The increased impedance can impair ion conductivity, enhance electron tunneling and result in Li metal accumulation at the interface, promoting dendrite growth and the formation of dead Li.[4] The minimal changes observed during cycling indicate intimate contact between the interlayer and electrolyte, as well as enhanced interfacial compatibility. It has been determined that the charge transfer resistance (R_{ct}) in the low-frequency range reflects the Li^+ solvation and desolvation dynamics, while the high-frequency range is associated with the impedance of the SEI (R_{SEI}).[5] The R_{SEI} values remain consistent throughout the cycling in the high-frequency region, indicating the absence of dead Li and the stability of the SEI, which ensures the steady operation of the Li@PZ-CHPT||LFP full cell.

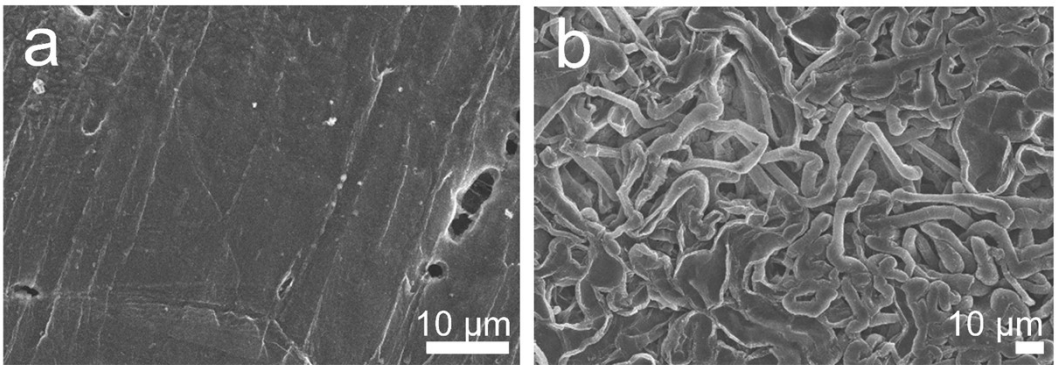

Fig. S19 Plane SEM scans of bare Li after (a) the 1st cycle and (b) the 100th cycle.

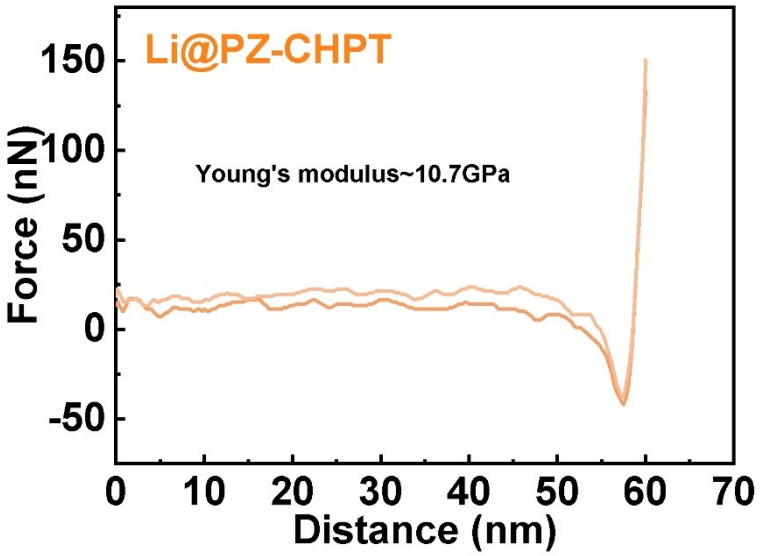

Fig. S20 AFM nanoindentation testing of PZ-CHPT@Li.

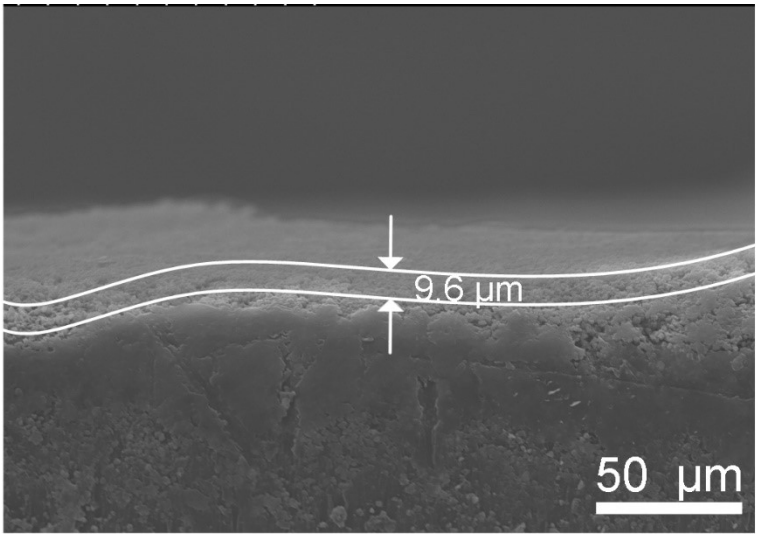

Fig. S21 Cross-sectional morphologies of Li@PZ-CHPT. Previous studies on covalent organic polymer-based artificial SEI layers have indicated that an optimal thickness generally lies within the range of 8–16 μm.[6] This range is recognized to balance satisfactory mechanical robustness for dendrite suppression with low ionic transport resistance.

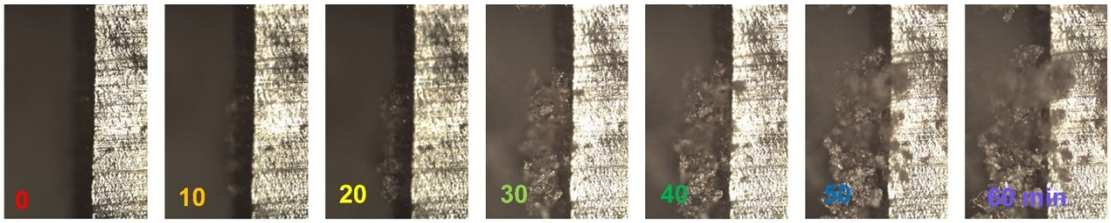

Fig. S22 *In-situ* OM images of Li deposition on bare Li.

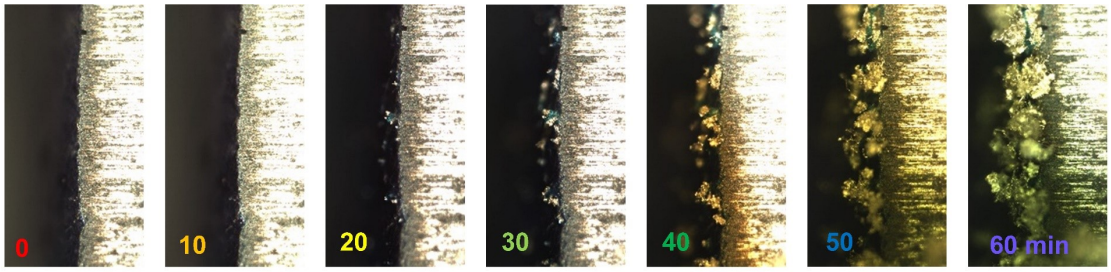

Fig. S23 *In-situ* OM images of Li deposition on Li@PZ-CHPD.

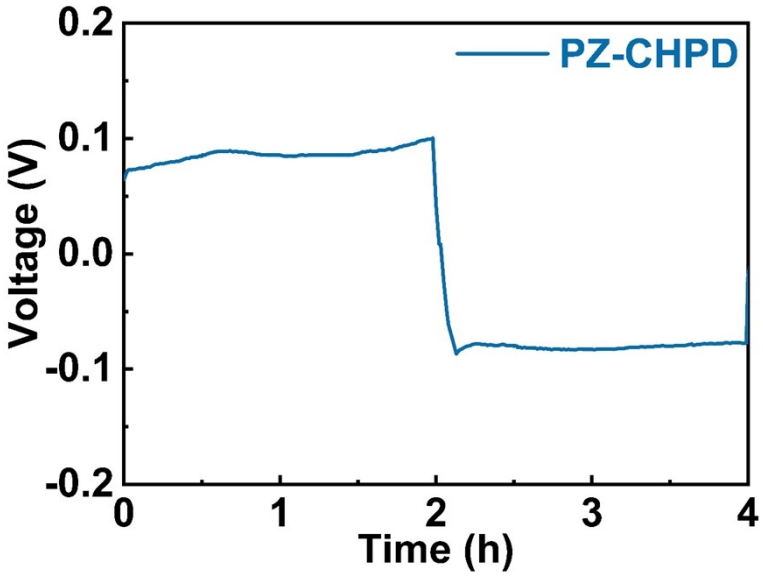

Fig. S24 Time-voltage plot of Li||Li symmetric battery based on PZ-CHPD.

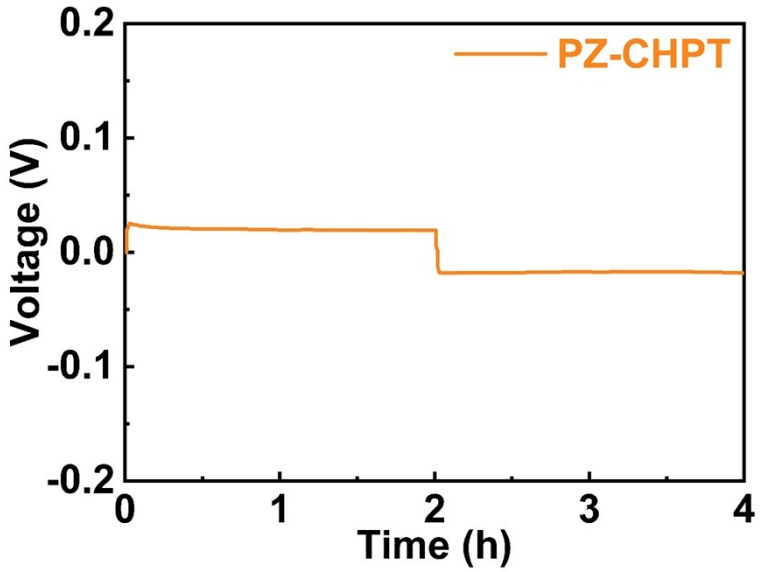

Fig. S25 Time-voltage plot of Li||Li symmetric battery based on PZ-CHPT.

Table S1. Comparison of plating/stripping life between this work and previous works of COFs.

Material	Potential Hysteresis (mV)	Current/ Capacity Density (mA cm^{-2}, mAh cm^{-2})	Cycling Lifespan (h)	Ref
PZ-CHPT	**23.5**	**3, 1**	**3200**	**This work**
	32.4	**5, 1**	**2800**	**This work**
	43.8	**10, 1**	**1300**	**This work**
BDTFP-COF	**24.9**	**1, 1**	**300**	[7]
TpTG COF	**11.0**	**1, 1**	**1800**	[8]
TpBpy-COF	**~20.0**	**1, 1**	**600**	[9]
$COF_{TAPB-PDA}$	**~32**	**1, 1**	**400**	[10]
S-COF	**20.2**	**4, 2**	**2400**	[11]
HS-POP	**＜30.0**	**0.5, 1**	**2400**	[12]
PA-COF	**15.0**	**5, 5**	**1000**	[13]
HAHATN-PMDA-COF	**15.0**	**0.5, 1**	**600**	[14]
G@COF-1	**~30.0**	**1, 1**	**300**	[15]
ACOF	**66.0**	**1, 1**	**600**	[16]
AQ-Si-COFs	**15.0**	**0.015 , 0.015**	**1000**	[17]
COF TpTt	**14.0**	**1, 1**	**2450**	[18]
CTF-LiI	**~80.0**	**1, 1**	**1400**	[19]
DCP-CTF	**25.0**	**1, 1**	**2000**	[20]
ivCOF-FSI	**30.0**	**2, 2**	**400**	[21]

REFERENCES

1. B. Delley, From Molecules to Solids with the DMol^3 Approach, *J. Chem. Phys.*, 2000, **113**, 7756-7764.
2. J. P. Perdew, K. Burke and M. Ernzerhof, Generalized Gradient Approximation Made Simple, *Phys. Rev. Lett.*, 1996, **77**, 3865-3868.
3. S. Grimme, Semiempirical GGA-Type Density Functional Constructed with A Long-Range Dispersion Correction, *J. Comput. Chem.*, 2006, **27**, 1787-1799.
4. X. Zhang, S. Wang, C. Xue, C. Xin, Y. Lin, Y. Shen, L. Li and C.-W. Nan, Self-Suppression of Lithium Dendrite in All-Solid-State Lithium Metal Batteries with Poly(vinylidene difluoride)-Based Solid Electrolytes, *Adv. Mater.*, 2019, **31**, 1806082.
5. B. Ma, H. Zhang, R. Li, S. Zhang, L. Chen, T. Zhou, J. Wang, R. Zhang, S. Ding, X. Xiao, T. Deng, L. Chen and X. Fan, Molecular-docking electrolytes enable high-voltage lithium battery chemistries, *Nat. Chem.*, 2024, **16**, 1427-1435.
6. X. M. Lu, Y. N. Cao, Y. Sun, H. C. Wang, W. W. Sun, Y. Xu, Y. Wu, C. Yang and Y. Wang, sp-Carbon-Conjugated Organic Polymer as Multifunctional Interfacial Layers for Ultra-Long Dendrite-Free Lithium Metal Batteries, *Angew. Chem. Int. Ed.*, 2024, **63**, e202320259.
7. X. Y. Ni, J. Liu, H. Q. Ji, L. B. Chen, T. Qian and C. L. Yan, Ordered Lithium Ion Channels of Covalent Organic Frameworks with Lithiophilic Groups Enable Uniform and Efficient Li Plating/Stripping, *J. Energy Chem.*, 2021, **61**, 135-140.
8. Y. R. Zhang, W. B. Wang, M. L. Hou, Y. T. Zhang, Y. Y. Dou, Z. H. Yang, X. Y. Xu, H. N. Liu and S. L. Qiao, Self-Exfoliated Covalent Organic Framework Nano-Mesh Enabled Regular Distribution for Stable Lithium Metal, *Energy Storage Mater.*, 2022, **47**, 376-385.
9. K. S. Oh, S. Park, J. S. Kim, Y. Yao, J. H. Kim, J. Guo, D. H. Seo and S. Y. Lee, Electrostatic Covalent Organic Frameworks as On-Demand Molecular Traps for High-Energy Li Metal Battery Electrodes, *ACS Energy Lett.*, 2023, **8**, 2463-2474.
10. D. D. Chen, S. Huang, L. Zhong, S. J. Wang, M. Xiao, D. M. Han and Y. Z. Meng, In Situ Preparation of Thin and Rigid COF Film on Li Anode as Artificial Solid Electrolyte Interphase Layer Resisting Li Dendrite Puncture, *Adv. Funct. Mater.*, 2020, **30**, 1907717.
11. W. B. Wang, Z. H. Yang, Y. T. Zhang, A. P. Wang, Y. R. Zhang, L. L. Chen, Q. Li and S. L. Qiao, Highly Stable Lithium Metal Anode Enabled by Lithiophilic and Spatial-Confined Spherical-Covalent Organic Framework, *Energy Storage Mater.*, 2022, **46**, 374-383.
12. Y. T. Zhang, Z. H. Yang, Y. Y. Dou, W. B. Wang, Y. R. Zhang, A. P. Wang, X. J. Zhang, X. M. Guo and S. L. Qiao, Hollow Spherical Organic Polymer Artificial Layer Enabled Stable Li Metal Anode, *Chem. Eng. J.*, 2022, **442**, 136155.
13. G. H. Li, Y. Yang, J. C. Cai, T. Wen, L. C. Zhuang, X. Y. Huang, Y. P. Cai and X. J. Hong, Lithiophilic Aromatic Sites and Porosity of COFs for a Stable Lithium Metal Anode, *ACS Appl. Energy Mater.*, 2022, **5**, 13554-13561.
14. X. Y. Wu, S. Q. Zhang, X. Y. Xu, F. X. Wen, H. W. Wang, H. Z. Chen, X. L. Fan

and N. Huang, Lithiophilic Covalent Organic Framework as Anode Coating for High-Performance Lithium Metal Batteries, *Angew. Chem. Int. Ed.*, 2024, **63**, e202319355.
15. Y. W. Song, P. Shi, B. Q. Li, X. Chen, C. X. Zhao, W. J. Chen, X. Q. Zhang, X. Chen and Q. Zhang, Covalent Organic Frameworks Construct Precise Lithiophilic Sites for Uniform Lithium Deposition, *Matter*, 2021, **4**, 253-264.
16. X. R. Li, Y. Tian, L. Shen, Z. B. Qu, T. Q. Ma, F. Sun, X. Y. Liu, C. Zhang, J. Q. Shen, X. Y. Li, L. N. Gao, S. X. Xiao, T. F. Liu, Y. Liu and Y. F. Lu, Electrolyte Interphase Built from Anionic Covalent Organic Frameworks for Lithium Dendrite Suppression, *Adv. Funct. Mater.*, 2021, **31**, 2009718.
17. C. Li, D. D. Wang, G. Ho, Z. Y. Zhang, J. Huang, K. T. Bang, C. Y. Lau, S. Y. Leu, Y. M. Wang and Y. Kim, Anthraquinone-Based Silicate Covalent Organic Frameworks as Solid Electrolyte Interphase for High-Performance Lithium-Metal Batteries, *J. Am. Chem. Soc.*, 2023, **145**, 24603-24614.
18. Z. H. Li, W. Y. Ji, T. X. Wang, Y. R. Zhang, Z. Li, X. S. Ding, B. H. Han and W. Feng, Guiding Uniformly Distributed Li-Ion Flux by Lithiophilic Covalent Organic Framework Interlayers for High-Performance Lithium Metal Anodes, *ACS Appl. Mater. Interfaces*, 2021, **13**, 22586-22596.
19. Y. X. Zheng, S. X. Xia, F. Dong, H. Sun, Y. P. Pang, J. H. Yang, Y. Z. Huang and S. Y. Zheng, High Performance Li Metal Anode Enabled by Robust Covalent Triazine Framework-Based Protective Layer, *Adv. Funct. Mater.*, 2021, **31**, 2006159.
20. X. D. Li, Y. T. Zhang, Y. Y. Dou, Z. Y. Zhao, X. Y. Fan and H. C. Jiang, Nanoporous Triazine-Framework-Assembled Electrolyte Interphase Layer as a Lithiophilic Gridding for Uniform Lithium Deposition and Dendrite Inhibition, *ACS Applied Nano Mater.*, 2024, **7**, 2825-2835.
21. W. F. Zhang, G. X. Jiang, W. W. Zou, L. H. Zhang, S. L. Li, S. G. Qi, X. J. Wang, Z. M. Cui, H. Y. Song, L. Du and Z. X. Liang, Ionic Covalent Organic Frameworks Triggered Efficient Synergy: Li Plus De-Solvation and the Formation of LiF-Rich Interphase, *J. Power Sources*, 2022, **548**, 232001.